Proceedings of the ASME 2023
International Design Engineering Technical Conferences and
Computers and Information in Engineering Conference
IDETC/CIE2023
August 20-23, 2023, Boston, Massachusetts

DETC2023- 117179

MODELING AND ANALYSIS OF A THIN PLATE WITH MULTIPLE HARMONIC EXCITATIONS FOR VIBROTACTILE TOUCH DISPLAY APPLICATIONS

Santosh Mohan Rajkumar
Miami University
Oxford, OH

Kumar Vikram Singh
Miami University
Oxford, Ohio

Jeong-Hoi Koo
Miami University
Oxford, Ohio

Tae-Heon Yang
Korea National University of Transportation,
Chungju-si, Korea

ABSTRACT

Touchscreen devices have become increasingly common in our daily lives. Although smaller touchscreen devices provide sufficient user interaction with meaningful tactile feedback, larger touch devices have the potential to offer a range of tactile stimulation. Previous research on large touch surface vibrotactile localization has utilized numerous actuators and traditional rigid boundary conditions. However, the possibility of localized haptic rendering using multi-frequency excitations is not explored for large rectangular touch surfaces. This study focuses on developing a finite element model of a large touch surface along with a limited number of electrostatic vibration actuators placed at different spatial locations and analyzing the vibrotactile response produced by various combinations of actuators with different frequencies and amplitudes. The effect of the number of actuators and their placement for rendering haptic feedback on the touch surface is explored. Statistical analysis is presented using model simulations to find out a suitable way of actuator placement which is otherwise cumbersome when chosen arbitrarily on a practical device. The effect of the mechanical property of the actuators on the haptic rendering is also explored. Finally, the possibility of localized haptic rendering by switching between actuator frequencies and actuation positions on the touch surface is demonstrated.

Keywords: haptics, vibrotactile feedback, large touchscreen, vibration analysis, multi-frequency device, finite element

1. INTRODUCTION

The advancement of haptic technology has transformed how we interact with computers and digital devices. Touchscreen displays (TSDs) are becoming increasingly popular in modern electronic devices due to their versatility and ability to provide interaction modes beyond audio and visual means, such as haptic and gesture modes [1]. Vibrotactile-based haptic actuation methods for TSDs are commercially preferred due to the bulky nature of equipment needed for kinesthetic haptic feedback [2]. Large touchscreen displays (TSDs) with a size of 12 inches or more are becoming increasingly popular in various fields. The automotive industry uses them for infotainment systems and center consoles [3]. In the entertainment sector, they are utilized in virtual reality (VR) and immersive gaming [4]. Additionally, large TSDs find applications in interactive education and training, including tablet-based learning for children [5], interactive tabletop medical training [6], and digital musical instruments [7]. These displays can also serve as assistive technologies for people with impaired vision and hearing disorders [8].

Commercially available large TSDs present a significant issue due to the lack of haptic feedback or inadequate feedback compared to the small TSDs found in mobile devices [9]. The absence of meaningful haptic feedback in large TSDs can negatively impact the user experience by reducing functionality and input accuracy [10]. In the case of automotive center consoles, large TSDs without haptic feedback can lead to driver distraction and a sense of unfamiliarity with non-physical controls [3]. Haptic feedback is necessary for digital musical instruments that use large touch surfaces to improve performance and enable people with hearing or visual impairments to use the instrument [11]. As a result, there is an increasing demand for large TSDs to include haptic feedback.

The limited availability of vibration actuators that can provide tactile feedback for large touchscreen displays significantly contributes to the lack of haptic feedback in such displays [12]. To make an actuator suitable for large TSDs, it should have several essential features such as quick response

time, minimal residual vibrations, low energy consumption, high vibration intensity, and appropriate size [13]. Electrostatic resonant actuators (ERAs), which are modified dual-electrode electrostatic actuators, are found to be suitable for haptic rendering on large TSDs [12][14][15]. Even with the use of a suitable vibration actuator type, dead zones or locations with no haptic feedback often exist on large TSDs due to the use of conventional rigid boundary conditions. Therefore, this study uses spring-damper boundary conditions to facilitate localized vibrotactile rendering based on the findings in [13]. Generating localized tactile feedback in large TSDs is still challenging despite the availability of suitable vibrotactile actuators and boundary conditions, owing to the difficulty in controlling waves that travel through them [10]. Localized haptic sensations in large TSDs are particularly sought after in various applications, including multi-user tabletop medical training, multi-segment automotive center consoles, interactive education, multi-touch haptics, virtual reality (VR), and immersive gaming.

Existing localized haptic rendering methods for large TSDs, such as eigenfunction superposition [16], time reversal wave focusing [17], [18], vibrotactile confinement [19], inverse filter method [20], and superimposition of vibration modes [21], [22] utilize many actuators. Due to size limitations in digital devices and instrument packaging, it is not preferable to utilize numerous actuators for haptic rendering on TSDs. Localized haptic rendering on large TSDs using a limited number of actuators is discussed in [13], [14] for a special kind of bar-type display. The use of a limited number of actuators for localized haptic rendering on large tactile sensation devices is explored in references [13] and [14], specifically for a type of bar-shaped display. There is a lack of research in the literature on localized haptic rendering using a limited number of vibration actuators for general-purpose rectangular TSDs.

The ability to create localized vibrotactile feedback on large TSDs with a limited number of actuators depends on factors such as the type of actuators used, the type of boundaries selected, the type of excitations, and the placement of the actuators [13]. However, physically constructing different large touch-sensitive devices with varying configurations of these factors is impractical. To address this issue, simulation models for large touch-sensitive devices need to be developed to explore localized vibrotactile feedback that can aid in optimizing the design of the TSD system. These models also allow for the extension of haptic rendering methods to different materials and actuators and better localization. Finite element modeling has been used to simulate touch surfaces with piezo actuators [23]–[26], but these studies have focused on generating maximum vibration amplitude rather than localized feedback. Comprehensive finite-element modeling for a special type of bar-shaped TSD is discussed in [13], [14] using ERAs for localized haptic rendering. However, there is a lack of studies on localized haptic rendering on large rectangular/general-purpose TSDs.

As previously discussed, there is a shortage of appropriate actuators for providing haptic feedback on large touchscreen displays (TSDs) due to the difficulty of implementing rigid boundary conditions. Creating localized haptic feedback on a large TSD with a limited number of suitable actuators and boundary conditions is also challenging, and this area has not been explored much. Therefore, there is a need to develop mechanical models of large TSDs to explore localized haptic rendering with a limited number of suitable actuators. A similar attempt was presented in [4] which focused on a bar-type touch display. This study proposes a finite element (FE) model of a large rectangular touch surface with a limited number of electrostatic resonating actuators (ERAs) placed at different locations. The model is developed in MATLAB using the Reissner-Mindlin thin-plate theory. Some advantages of developing an in-house model in MATLAB compared to conventional CAD software are as follows,

- An in-house model can offer more flexibility and customization options.
- Customized computationally efficient solvers can be implemented.
- Possible integration with data analytics software, AI/ML libraries, and other programming interfaces which can provide convenient data manipulation, optimization, statistical analysis, and simulation.

This study presents statistical visualization of vibrotactile feedback information computed using the in-house FE model for a rectangular large TSD with ERAs to determine a suitable number of ERAs and their placement to achieve higher vibrotactile intensity. The vibrotactile intensities are represented as peak accelerations at different spatial locations of the TSD in the unit of g ($1g = 9.8\ m/s^2$). Using a few numerical simulation examples of the FE model, it is also shown that ERAs' placement affects the vibrotactile rendering pattern on a large TSD and the actuator's mechanical properties like the stiffness affect the vibrotactile intensity. Further, this study showcases the ability to achieve localized haptic rendering on a large TSD, which involves the production of a variety of haptic sensations that are localized to specific regions of the touch surface. With multiple ERAs, it has been established using numerical simulation of the FE model of the TSD that localized haptic rendering can be achieved by strategically switching between different excitation frequencies of the ERAs. This finding can lead to controlled localized haptic rendering on large TSDs by switching between the excitation frequencies of the actuators and their activation patterns.

The organization of this paper is as follows: section 2 introduces the proposed rectangular TSD system with ERAs followed by its FE modeling and analysis, section 3 provides results and discussion, and section 4 is the conclusion.

2. MODELING AND ANALYSIS APPROACH

The touch surface considered here is a 15-inch uniform rectangular general-purpose one with a 4:3 aspect ratio with the dimensions as shown in Figure 1. The touch surface is connected directly to multiple dual-electrode electrostatic resonating actuators (ERAs), forming a structure as shown in Figure 2(b). The touch surface is not fixed on any ends and the stiffness-

damping of the ERAs provides support at the boundaries The ERAs generate sinusoidal displacements that transmit to the touch bar through their connections and the excitation frequencies can be independently controlled for each ERA. The touch surface is bolted to the central hole of the ERAs, and the stiffness and damping of the actuators get reflected at the boundary through the bolt. For this study, we consider that each ERA's stiffness, damping, and displacement amplitude are the same. Each ERA's stiffness, damping, and displacement amplitude are based on the dynamic characterization presented in [15]. Here we consider, k_b as the actuator stiffness, m_b as the mass of the bolt connecting each ERA to the touch surface, c as the damping coefficient of each ERA with damping ratio ζ, and α as the maximum amplitude of displacement input from the actuator.

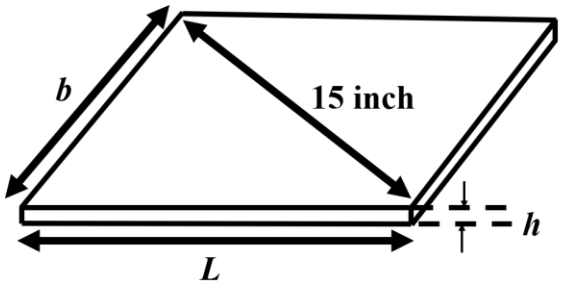

FIGURE 1: THE DIMENSIONS OF THE TOUCH SURFACE CONSIDERED

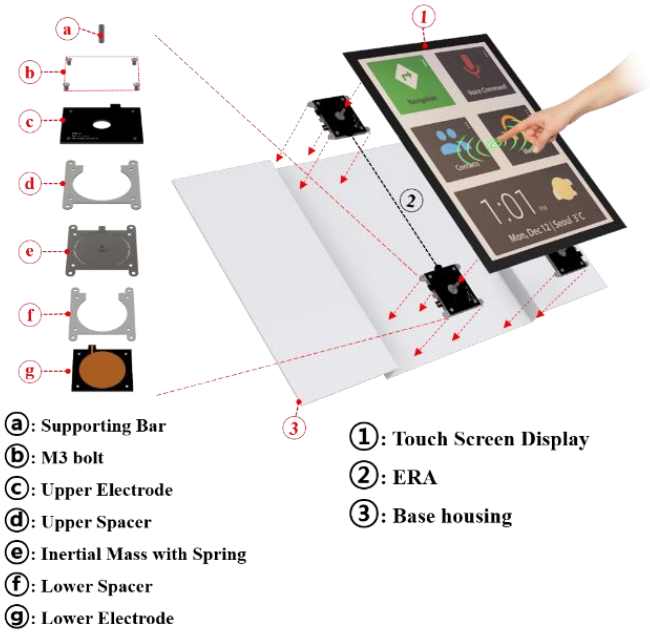

FIGURE 2: TOUCH SURFACE WITH FOUR ELECTROSTATIC RESONATING ACTUATORS: CONCEPTUAL ILLUSTRATION OF THE SYSTEM

2.1 Modeling of the touch surface as a thin plate

The touch surface is modeled as a thin plate using the Reissner-Mindlin plate theory [27]. The Reissner-Mindlin theory is selected due to its relevance to thin as well as moderately thick plate surfaces [28]. We use this theory to derive the governing equation of motion of the plate-type touch surface rendering vibrotactile feedback. The Reissner-Mindlin theory in 2D uses the middle plane model, and it is assumed that there is no in-plane deformation in the middle plane and that the transverse deflection $w(x,y,t)$ is negligible compared to the plate thickness. Unlike classical Kirchhoff plate theory, the Reissner-Mindlin theory considers transverse shear deformation. Due to transverse shear, the bending deformations are not directly related to the slopes of the transverse deflection $w(x,y,t)$. This implies that the rotations of the plate cross-section due to bending are not related to the spatial derivatives of the transverse displacements $\partial w/\partial x$, $\partial w/\partial y$ and are independent variables β_x, β_y. The bending deformations due to transverse shear from figure 4 are given as,

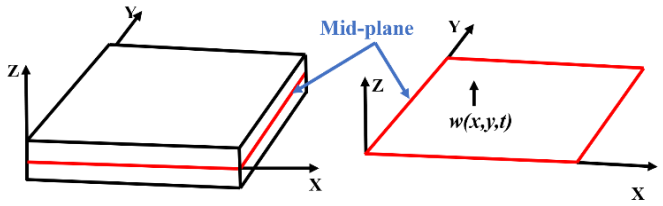

FIGURE 3: THE COORDINATE SYSTEM AND 2D MIDDLE PLANE OF THE TOUCH SURFACE AS A THIN PLATE

$$u = -z\beta_x, \quad v = -z\beta_y \tag{1}$$

We assume a linear homogeneous material for the touch surface with E being the elastic modulus, G being the shear modulus, ρ being density, and υ being Poisson's ratio.

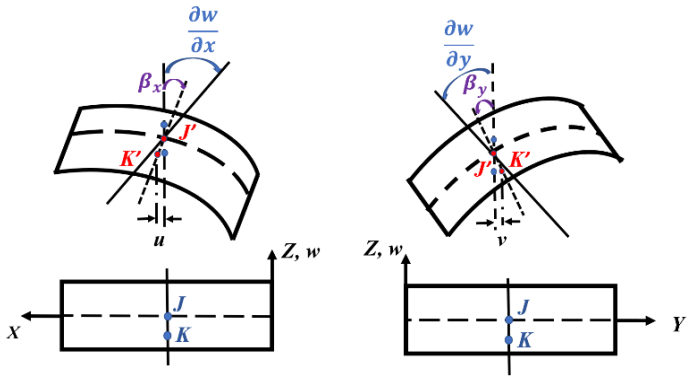

FIGURE 4: PLATE BENDING DEFORMATIONS DUE TO TRANSVERSE SHEAR

The strains on the X-Y plane are computed using (1) as,

$$\varepsilon_x = \frac{\partial u}{\partial x} = -z\frac{\partial \beta_x}{\partial x}, \quad \varepsilon_y = \frac{\partial v}{\partial y} = -z\frac{\partial \beta_y}{\partial y}$$
$$\gamma_{xy} = \frac{\partial u}{\partial y} + \frac{\partial v}{\partial x} = -z\left(\frac{\partial \beta_x}{\partial y} + \frac{\partial \beta_y}{\partial x}\right) \tag{2}$$

The transverse shear strains are computed as,

$$\gamma_{xz} = \frac{\partial w}{\partial x} - \beta_x, \qquad \gamma_{yz} = \frac{\partial w}{\partial y} - \beta_y \tag{3}$$

Using (2) & (3) various stresses are computed as,

$$\begin{bmatrix}\sigma_x \\ \sigma_y \\ \tau_{xy}\end{bmatrix} = \begin{bmatrix} E/(1-\upsilon^2) & \upsilon E/(1-\upsilon^2) & 0 \\ \upsilon E/(1-\upsilon^2) & E/(1-\upsilon^2) & 0 \\ 0 & 0 & G \end{bmatrix}\begin{bmatrix}\varepsilon_x \\ \varepsilon_y \\ \gamma_{xy}\end{bmatrix},$$
$$\tau_{xz} = G\left(\frac{\partial w}{\partial x} - \beta_x\right), \qquad \tau_{yz} = G\left(\frac{\partial w}{\partial y} - \beta_y\right) \tag{4}$$

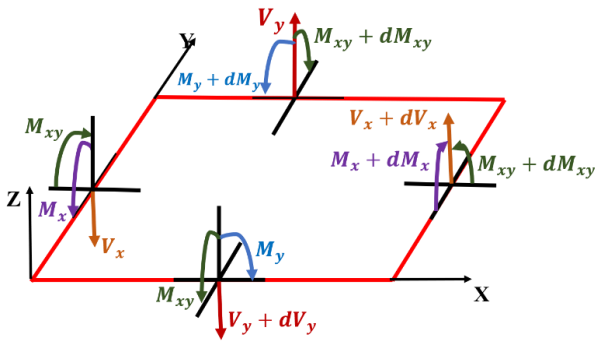

FIGURE 5: FREE BODY DIAGRAM OF THE MIDDLE PLANE OF THE PLATE MODEL

Using (4) the resulting moment and shear force intensities, as shown in figure 5, are computed as,

$$\begin{bmatrix}M_x \\ M_y \\ M_{xy}\end{bmatrix} = -D\begin{bmatrix}1 & \upsilon & 0 \\ \upsilon & 1 & 0 \\ 0 & 0 & (1-\upsilon)/2\end{bmatrix}\begin{bmatrix}\frac{\partial \beta_x}{\partial x} \\ \frac{\partial \beta_y}{\partial y} \\ \frac{\partial \beta_x}{\partial y} + \frac{\partial \beta_y}{\partial x}\end{bmatrix} = -D\mathbf{C}_b\boldsymbol{\Theta}_b \tag{5}$$

$$\begin{bmatrix}V_x \\ V_y\end{bmatrix} = \Upsilon Gh\begin{bmatrix}\frac{\partial w}{\partial x} - \beta_x \\ \frac{\partial w}{\partial y} - \beta_y\end{bmatrix} = \Upsilon Gh\boldsymbol{\Theta}_s \tag{6}$$

Where,

$$D = \frac{Eh^3}{12(1-\nu^2)} \tag{7}$$

is the flexural rigidity of the touch surface material and Υ is the shear correction factor.

The weak form of the touch surface as a thin plate can be derived using the weighted residual of the equilibrium of forces, equilibrium of moments about the X-axis, and equilibrium of moments about the Y-axis. The weighting functions used are $\bar{w}_f$, $\bar{w}_{mx}$, and $\bar{w}_{my}$, respectively, for the three equilibrium equations. Considering f as the load on the touch surface, the weighted residual equation is expressed as,

$$\iint_A \left[\begin{array}{l}\left(\frac{\partial V_X}{\partial x} + \frac{\partial V_y}{\partial y} + f\right)\bar{w}_f + \left(V_x - \frac{\partial M_x}{\partial x} - \frac{\partial M_{xy}}{\partial y}\right)\bar{w}_{mx} \\ \qquad + \left(V_y - \frac{\partial M_{xy}}{\partial x} - \frac{\partial M_y}{\partial y}\right)\bar{w}_{my}\end{array}\right] dA = 0 \tag{8}$$

Using equations (5) & (6) in (8), considering Γ being the total boundary, ignoring boundary moments for touch surface application, and using Green's theorem and some manipulations, the weak form of the thin plate model of the touch surface can be expressed as,

$$\iint_A \bar{\boldsymbol{\Theta}}_s^T \Upsilon Gh\boldsymbol{\Theta}_s dA + D\iint_A \bar{\boldsymbol{\Theta}}_b^T \mathbf{C}_b\boldsymbol{\Theta}_s dA = \iint_A f\bar{w}_f dA + \int_\Gamma V_n \bar{w}_f d\Gamma \tag{9}$$

Where, $\bar{\boldsymbol{\Theta}}_s$ and $\bar{\boldsymbol{\Theta}}_b$ are shear and bending weighting vectors respectively, and V_n represents the boundary shear forces.

2.2 Finite element (FE) modeling of the touch surface

For finite element modeling of the touch surface, we consider it to be c omposed of n_{el} rectangular four-node elements with 3 degrees of freedom (DoF) at each node resulting in a total of 12 DoF for each element. Each node i within an element has a transverse displacement w_i^e and the rotations β_{xi}^e, β_{yi}^e due to bending resulting in a vector of displacements and rotations (degrees of freedom) shown below,

$$\mathbf{d}^e = [w_1^e \quad \beta_{x1}^e \quad \beta_{y1}^e \quad w_2^e \quad \beta_{x2}^e \quad \ldots]^T \tag{10}$$

For four-node rectangular elements, we use interpolation functions $\mathbf{N} = [\mathbf{N_1}\ \mathbf{N_2}\ \mathbf{N_3}\ \mathbf{N_4}]^T$ to interpolate displacements and rotations within the element as shown below,

$$\mathbf{w}^e = \begin{bmatrix}\mathbf{N}_1 & 0 & 0 & \mathbf{N}_2 & \ldots\end{bmatrix}\begin{bmatrix}w_1^e \\ \beta_{x1}^e \\ \beta_{y1}^e \\ w_2^e \\ \vdots\end{bmatrix} = \mathbf{N}_d{}^T\mathbf{d}^e \tag{11}$$

$$\boldsymbol{\beta}_x^e = \begin{bmatrix} 0 & \mathbf{N}_1 & 0 & 0 & \ldots \end{bmatrix} \begin{bmatrix} w_1^e \\ \beta_{x1}^e \\ \beta_{y1}^e \\ w_2^e \\ \vdots \end{bmatrix} = \mathbf{N}_{rx}{}^T \mathbf{d}^e \tag{12}$$

$$\boldsymbol{\beta}_y^e = \begin{bmatrix} 0 & 0 & -\mathbf{N}_1 & 0 & \ldots \end{bmatrix} \begin{bmatrix} w_1^e \\ \beta_{x1}^e \\ \beta_{y1}^e \\ w_2^e \\ \vdots \end{bmatrix} = \mathbf{N}_{ry}{}^T \mathbf{d}^e \tag{13}$$

We write the elemental shear and bending quantities as shown below.

$$\boldsymbol{\Theta}_s = \mathbf{B}_s{}^T \mathbf{d}^e = \begin{bmatrix} \dfrac{\partial \mathbf{N}_1}{\partial x} & 0 & \mathbf{N}_1 & \dfrac{\partial \mathbf{N}_2}{\partial x} & \ldots \\ \dfrac{\partial \mathbf{N}_1}{\partial y} & -\mathbf{N}_1 & 0 & \dfrac{\partial \mathbf{N}_2}{\partial y} & \ldots \end{bmatrix} \mathbf{d}^e \tag{14}$$

$$\boldsymbol{\Theta}_b = \mathbf{B}_b{}^T \mathbf{d}^e = \begin{bmatrix} 0 & 0 & \dfrac{-\partial \mathbf{N}_1}{\partial x} & 0 & \ldots \\ 0 & \dfrac{\partial \mathbf{N}_1}{\partial y} & 0 & 0 & \ldots \\ 0 & \dfrac{\partial \mathbf{N}_1}{\partial x} & \dfrac{-\partial \mathbf{N}_1}{\partial y} & 0 & \ldots \end{bmatrix} \mathbf{d}^e \tag{15}$$

The weak form for a rectangular element can be derived using (9) as,

$$\left(\kappa G h \int\int_A \mathbf{B}_s \mathbf{B}_s{}^T dA + D \int\int_A \mathbf{B}_b \mathbf{C}_b \mathbf{B}_b{}^T dA \right) \mathbf{d}^e = \int\int_A f^e \mathbf{N}_d dA + \int_\Gamma V_n^e \mathbf{N}_{d\Gamma} d\Gamma \tag{16}$$

From(16), the elemental shear and bending stiffness matrices are defined as,

$$\mathbf{K}_s^e = \kappa G h \int\int_A \mathbf{B}_s \mathbf{B}_s{}^T dA, \quad \mathbf{K}_b^e = D \int\int_A B_b \mathbf{C}_b B_b{}^T dA \tag{17}$$

The elemental forcing vector is defined as,

$$\mathbf{f}^e = \int\int_A f^e \mathbf{N}_d dA \tag{18}$$

The elemental mass matrix for a thin plate is derived using kinetic energy formulation as,

$$\mathbf{M}^{e/} = \int\int_A \mathbf{N}_A \mathbf{H} \mathbf{N}_A{}^T dA \tag{19}$$

Where,

$$\mathbf{N}_A = [\mathbf{N}_d \quad \mathbf{N}_{rx} \quad \mathbf{N}_{ry}]$$
$$\mathbf{H} = \rho \begin{bmatrix} h & 0 & 0 \\ 0 & h^3/12 & 0 \\ 0 & 0 & h^3/12 \end{bmatrix} \tag{20}$$

For the touch surface supported with spring-damper connection with the ERAs, the elemental boundary shear force can be expressed as,

$$V_n^e = n(m_b \ddot{\mathbf{w}}_\Gamma^e + c\dot{\mathbf{w}}_\Gamma^e + k_b \mathbf{w}^e{}_\Gamma) = n(m_b \mathbf{N}_{d\Gamma}{}^T \ddot{\mathbf{d}}^e + c\mathbf{N}_{d\Gamma}{}^T \dot{\mathbf{d}}^e + k_b \mathbf{N}_{d\Gamma}{}^T \mathbf{d}^e) \tag{21}$$

Here, n = $\begin{cases} 1 \text{ if } V_n^e \text{ is at the axes of the reference frame} \\ -1 \text{ if } V_n^e \text{ is not at the axes of the reference frame} \end{cases}$

Therefore, the elemental mass, stiffness, and damping matrices for the touch surface connected with ERAs can be expressed as,

$$\mathbf{M}^e = \mathbf{M}^{e/} - nm_b \int_\Gamma \mathbf{N}_{d\Gamma}{}^T \mathbf{N}_{d\Gamma} d\Gamma$$
$$\mathbf{K}^e = \mathbf{K}_b^e + \mathbf{K}_s^e - nk_b \int_\Gamma \mathbf{N}_{d\Gamma}{}^T \mathbf{N}_{d\Gamma} d\Gamma \tag{22}$$
$$\mathbf{C}^e = -nc \int_\Gamma \mathbf{N}_{d\Gamma}{}^T \mathbf{N}_{d\Gamma} d\Gamma$$

We can now compute the elemental mass, spring, and damper matrices using the following linear shape functions $\mathbf{N}$ in Gaussian co-ordinate system and using Gaussian integration

$$\mathbf{N} = \begin{bmatrix} \frac{1}{4}(1+\xi)(1+\eta) \\ \frac{1}{4}(1-\xi)(1+\eta) \\ \frac{1}{4}(1-\xi)(1-\eta) \\ \frac{1}{4}(1+\xi)(1-\eta) \end{bmatrix}. \tag{23}$$

Using a suitable assembly process for n_{el} finite elements, we obtain the global mass matrix $\mathbf{M}$, stiffness matrix $\mathbf{K}$, damping matrix $\mathbf{C}$, and external forces matrix $\mathbf{f}$ defining the following differential equation of motion for the touch surface actuated by the ERAs,

$$\mathbf{M}\ddot{\mathbf{d}}(t) + \mathbf{C}\dot{\mathbf{d}}(t) + \mathbf{K}\mathbf{d}(t) = \mathbf{f}(t) \tag{24}$$

Where, $\mathbf{d}$ is the vector containing the displacements and slopes at all the global nodes.

With multiple ERAs attached to the touch surface capable of exciting it sinusoidal displacements with different excitation

frequencies, the governing equation of motion of the touch surface in (24) for multi-frequency excitation can be expressed as,

$$\mathbf{M}\ddot{\mathbf{d}}(t)+\mathbf{C}\dot{\mathbf{d}}(t)+\mathbf{K}\mathbf{d}(t)=\sum_{i=1}^{m}\left(\mathbf{s}_i \sin\omega_i t+\mathbf{g}_i \cos\omega_i t\right) \quad (25)$$

Here, $\mathbf{s}_i$ and $\mathbf{g}_i$ are vectors of amplitudes of harmonic excitations at the $i-th$ degree of freedom. In order to compute tactile feedback at various positions on the touch surface, we need to calculate the solution to the system of differential equations described in(25). To accomplish this, we use an effective analytical solution method that provides the displacements and slopes for the different degrees of freedom of the finite element model. Equation (26) shows the results of this method for initially relaxed conditions. Further information on the derivation of the analytical solution method can be found in [14].

$$\mathbf{d}(t)=\sum_{i=1}^{m}\left(\mathbf{S}_i \cos\omega_i t+\mathbf{G}_i \sin\omega_i t\right) \quad (26)$$

Here, $\mathbf{S}_i$ and $\mathbf{G}_i$ describe harmonic motion with frequency ω_i at different degrees of freedom. The peak steady-state accelerations at different degrees of freedom of the touch surface is given as [14],

$$\boldsymbol{\varphi}(t)=-\sum_{i=1}^{m}\omega_i^2\left(\mathbf{S}_i \cos\omega_i t+\mathbf{G}_i \sin\omega_i t\right) \quad (27)$$

We compute the absolute value of the peak steady-state acceleration at any degree of freedom *k* of the touch surface as [14],

$$\boldsymbol{\varphi}_k == \sum_{i=1}^{m}\omega_i^2\sqrt{\left(S_k\right)_i^2+\left(G_k\right)_i^2} \quad (28)$$

The computed peak steady-state acceleration at different global nodes can be interpolated across each element using the shape function defined above to obtain vibrotactile response across the touch surface.

3. RESULTS AND DISCUSSION

We have developed an FE model of the touch surface with directly connected ERAs in MATLAB based on the formulation provided in the previous section. For validation purpose, we consider a homogeneous touch surface made of Aluminum with material properties $E=70\ GPa,\ \rho=2700\ kg/m^3,\ \upsilon=0.33$ and dimensions $L=12\ inch,\ b=9\ inch,\ h=1.5\ mm$. For preliminary verification, we construct the FE model of the touch surface considering simply-supported at all edges (SSSS), ignoring the ERAs. The analytical solution for the eigen frequencies of the simply supported touch surface as a thin plate is given as,

$$\omega_{ij}=\left(\left(\frac{j\pi}{b}\right)^2+\left(\frac{i\pi}{L}\right)^2\right)\sqrt{\frac{D}{\rho h}};\ \text{for } i,j=1,2,3,\ldots \quad (29)$$

The eigenfrequencies of the touch surface as a thin plate are also computed using the in-house FE model and a COMSOL CAD model (tetrahedral element with normal physics-controlled mesh). The results presenting the eigenfrequencies in Table 1 validate the efficacy of the in-house FE model. It is important to note that the COMSOL model computed eigen-frequencies are closer to the analytical values as the mesh is much finer in the COMSOL model compared to the in-house FE model. However, considering the computational efficiency of the in-house model (0.0254 m mesh size, 390 DoF), the percentage errors are reasonable when compared to the results from the analytical solution. Figure 6 depicts the mode shapes 1 and 2 computed using the in-house FE and COMSOL CAD models, showing agreement with the in-house FE model.

Table 1. Eigen Frequencies of SSSS the Aluminum Touch Surface

Mode Shape	Eigen Frequencies (Hz)			
	Analytical	COMSOL	In-house MATLAB*	% Error**
1	109.70	109.6	110.95	1.14
2	228.17	228.02	234.16	2.63
3	320.31	320.29	337.90	5.49
4	425.62	425.6	454.29	6.73
5	438.79	438.6	459.69	4.76

*Using mesh size of 0.0254m (12x 9 elements, 390 DoF)
** Comparing in-house model results with the analytical result

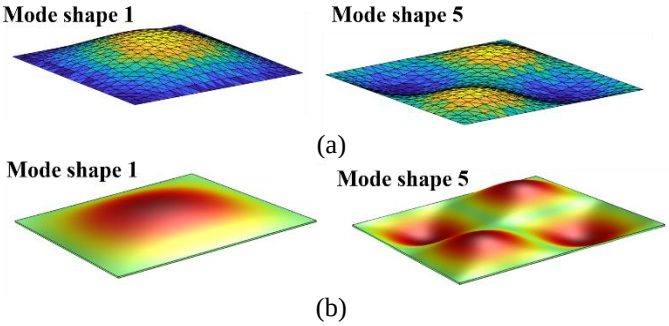

FIGURE 6: (a) MODE SHAPES 1 & 5 OF THE SSSS ALUMINUM TOUCH SURFACE FROM IN-HOUSE FE MODEL (b) MODE SHAPES 1 & 5 OF THE SSSS ALUMINUM TOUCH SURFACE FROM COMSOL MODEL

For further validation of our FE model, we consider a scenario where four ERAs are attached to each corner of the touch surface, providing spring-damper boundaries. For this analysis, we are ignoring the damping effects at the boundary. Eigen-frequencies for the touch surface with the four ERAs at the corner are computed using the in-house FE model (0.0254 m mesh size, 390 DoF) and a COMSOL CAD model (tetrahedral element with normal physics-controlled mesh). The computed eigen-frequencies are summarized in Table 2. The agreement of the in-house FE model with the COMSOL CAD model is evident

from Table 2. This validates our in-house FE model of the touch surface with ERAs.

Table 2. Eigen Frequencies of the Aluminum Touch Surface with 4 ERAs at the Corners

Mode Shape	Eigen Frequencies (Hz)		
	In-house MATLAB*	COMSOL	% Error
1	31.98	31.67	1
2	68.50	68.07	0.63
3	76.62	75.62	1.33
4	107.84	106.53	1.23
5	160.77	157.14	2.31

* Using mesh size of 0.0254m (12x 9 elements, 390 DoF)

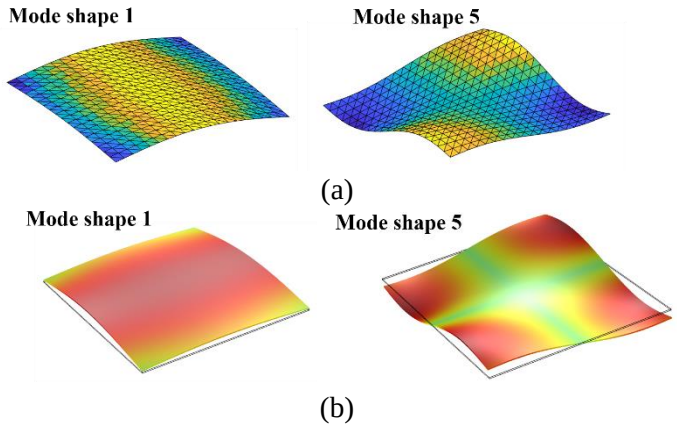

FIGURE 7: (a) MODE SHAPES 1 & 5 OF THE ALUMINUM TOUCH SURFACE WITH 4 ERAS AT THE CORNERS FROM IN-HOUSE FE MODEL (b) MODE SHAPES 1 & 5 OF THE ALUMINUM TOUCH SURFACE WITH 4 ERAS AT THE CORNERS FROM COMSOL MODEL

3.2 Effect of the number of actuators and their placement

To investigate how the number and placement of ERAs affect the touch surface's vibrotactile intensity, we should examine the highest acceleration amplitudes produced by sinusoidal excitations at frequencies that humans are most sensitive to in terms of tactile stimulation. However, physically testing the touch bar under various conditions is not feasible. Instead, we can utilize the suggested finite element model to statistically evaluate the touch surface's tactile response to different actuator configurations and placements. For this study, we consider that four ERAs are attached to the four different locations of the touch surface.

To study the effect of the number of actuators providing excitations to the touch surface, we consider two scenarios: first when one ERA is activated as shown in Figure 8, and second when two ERAs are activated as shown in Figure 9. It is worth noting that we are using four ERAs here and depending on the scenario, one or two ERAs are activated. Rest of the ERAs provide boundary supports only. We can also replace the non-activated ERAs with springs and dampers of similar mechanical properties for these two scenarios.

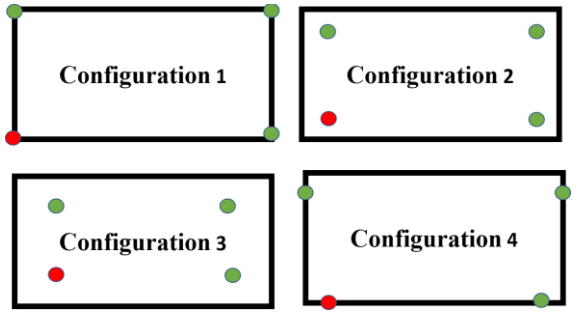

FIGURE 8: SCENARIO 1: DIFFERENT CONFIGURATIONS OF THE ERAS. (THE RED DOT REPRESENTS THE ERA THAT IS BEING ACTIVATED AND THE GREEN DOTS REPRESENTS THE ERAS PROVIDING BOUNDARY SUPPORTS ONLY)

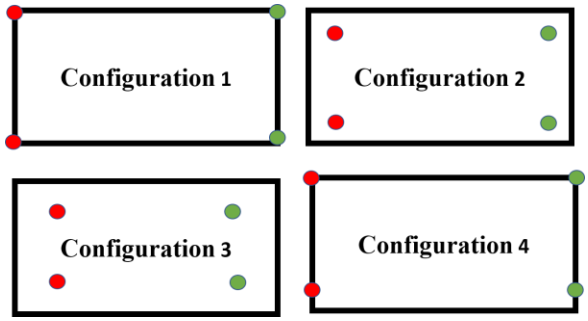

FIGURE 9: SCENARIO 2: DIFFERENT CONFIGURATIONS OF THE ERAS. (THE RED DOTS REPRESENT THE ERAS THAT ARE BEING ACTIVATED AND THE GREEN DOTS REPRESENTS THE ERAS PROVIDING BOUNDARY SUPPORTS ONLY)

For the two scenarios presented in Figure 8 & Figure 9, our aim is to find out the suitable configuration that provides the highest vibrotactile intensities at different spatial locations of the touch surface. For this purpose, considering maximum amplitude of the ERAs and 27 different excitation frequencies in the human haptic range, we computed peak vibrotactile accelerations throughout the surface using the FE model for each configuration of the two scenarios. For each configuration, we accumulate the peak accelerations across all frequencies and take the help of statistical visualization that shows their box plots. Figure 10 shows the box plots of peak accelerations for different configurations of scenario 1. We observe from Figure 10 that configuration 1 has higher median of peak accelerations compared to rest of the configurations. Therefore, for scenario 1, configuration 1 is clearly a suitable choice for greater vibrotactile intensity. Figure 11 shows the box plots of peak accelerations for different configurations of scenario 2. We observe from Figure 11 that configuration 1 & 4 have much higher median of peak accelerations compared to rest of the configurations. Configuration 4 has slightly higher median of peak accelerations than configuration 1. Therefore, for scenario 2, configuration 4 closely followed by configuration 1 are clearly suitable choices

for greater vibrotactile intensity. Further, we have observed from Figure 10 and Figure 11 that the use of two ERAs increases the vibrotactile intensities on the TSD significantly. Clearly, use of two actuators will be more suitable for effective haptic rendering. This statistical analysis can be extended to a greater number of scenarios depending on application areas and accordingly we can obtain suitable number of actuators and their placement for achieving higher vibrotactile intensity.

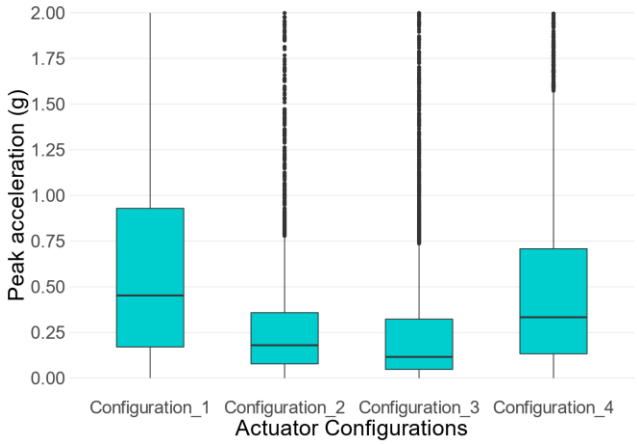

FIGURE 10: DISTRIBUTION OF CUMULATIVE PEAK ACCELERATIONS FOR DIFFERENT CONFIGURATION OF SCENARIO 1 WHEN ONE ERA IS ACTIVATED

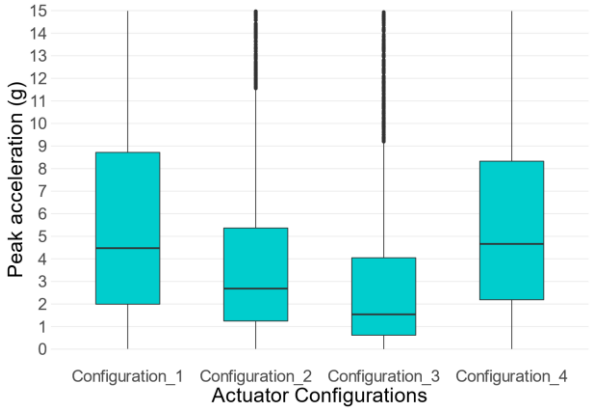

FIGURE 11: DISTRIBUTION OF CUMULATIVE PEAK ACCELERATIONS FOR DIFFERENT CONFIGURATION OF SCENARIO 2 WHEN TWO ERAS ARE ACTIVATED

Activation patterns of the ERAs for a particular number of them are found to be impacting the vibrotactile rendering pattern across the TSD. To corroborate this finding, in Figure 11, we have shown two cases utilizing two ERAs: ERAs diagonally opposite are activated and ERAs on the same edge are activated (both of them at 110 Hz frequency). We have observed a negligible change in maximum peak accelerations after obtaining numerical results for both the cases. In Figure 11, we observe that changing the actuator activation pattern neutralizes several zones of insignificant vibration (each node point shown by red colored x). This behavior implies that switching between actuators or changing the activation patterns of the ERAs can aid in localized vibrotactile feedback rendering.

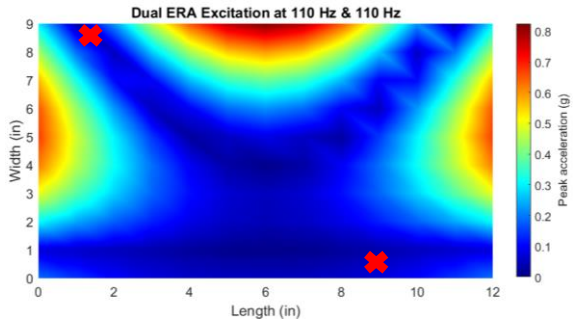

(a)

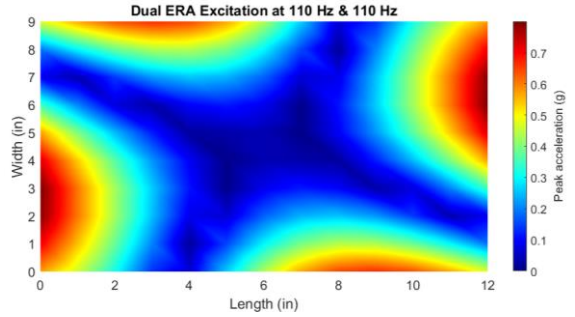

(b)

FIGURE 11: PEAK ACCELERATIONS COMPUTED ACROSS THE TOUCH SURFACE WHEN (a) TWO ERAS ON THE SAME EDGE ARE ACTIVATED (b) TWO ERAS AT THE DIAGONALLY OPPOSITE SIDES ARE ACTIVATED (BOTH AT 110 HZ) (X DENOTES A NODE POINT)

3.3 Effect excitation frequency and actuator stiffness

To study the effect of changing excitation frequencies on the rendered vibrotactile feedback for the TSD system, we considered excitations with two ERAs. The TSD is supported at the four corners with either an ERA or an inactive ERA/equivalent boundary support. Figure 12(a)-(f) shows the vibrotactile intensity throughout the TSD with the frequencies of excitation switched between the two active ERAs at the diagonally opposite corners. First, in Figure 12(a) the touch surface is excited with both the ERAs at 320 Hz, and three of the many node points are marked. When the excitation frequencies are switched to 300 Hz & 100 Hz as in Figure 12(b), the marked node points are nullified along with many other node points. Several other node points are observed at this excitation, and three of them are marked on Figure 12(b). Switching the excitation frequencies to 100 Hz & 300 Hz as in Figure 12(c) nullifies the marked nodes. In Figure 12(c), several other node points come up, and three of them are marked again. Again, we switch the excitation frequencies to 170 Hz for both the ERAs as in Figure 12(d), and the marked nodes got nullified with several other nodes coming up (two of them are shown). In Figure 12(e) the two nodes shown in Figure 12(d) got nullified as we switch the excitation frequencies to 250 Hz & 220 Hz. Finally, the nodes marked in Figure 12(e) got nullified as we switch to 150 Hz

frequencies for both the ERAs. In this way, by switching between the excitation frequencies, we can have localized vibrotactile haptic feedback on a large TSD.

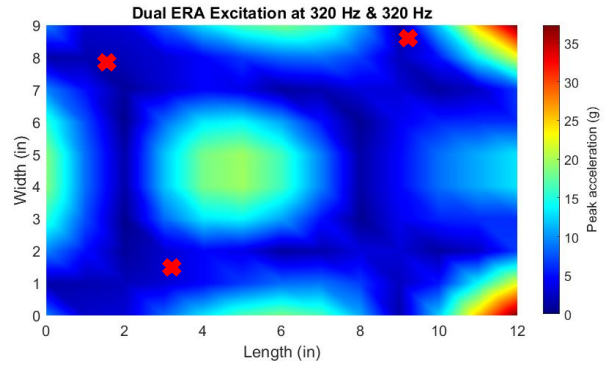

(a)

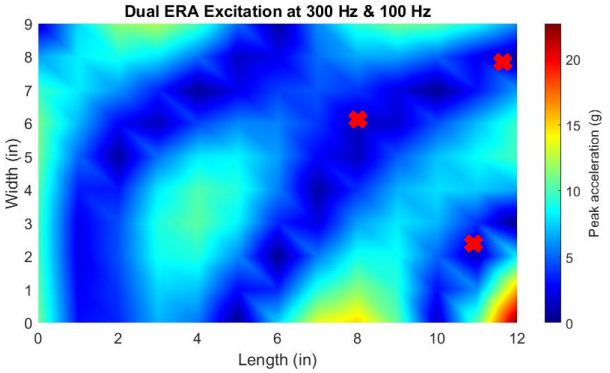

(b)

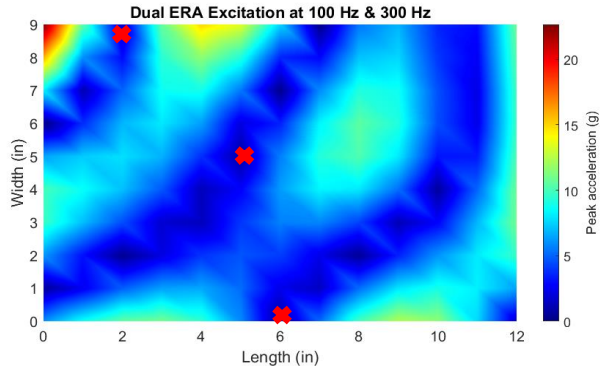

(c)

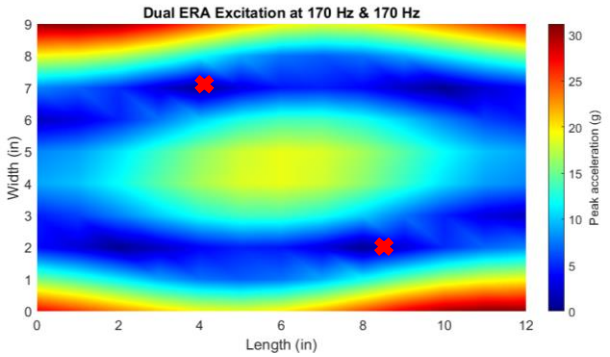

(d)

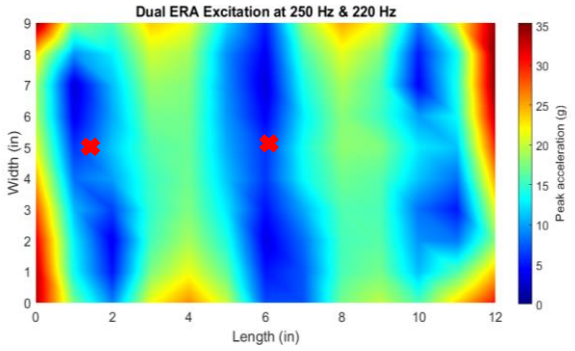

(e)

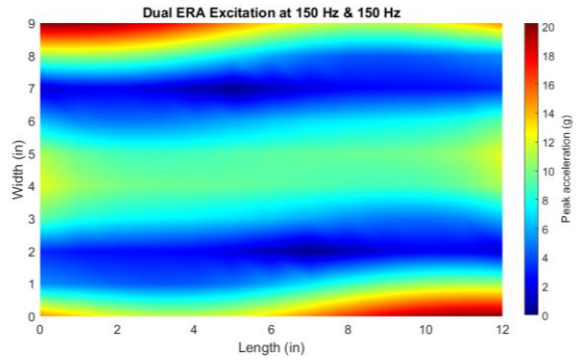

(f)

FIGURE 12: PEAK ACCELERATIONS COMPUTED ACROSS THE TOUCH SURFACE WHEN TWO ERAS AT DIAGONALLY OPPOSITE CORNERS ARE ACTIVATED & EXCITATION FREQUENCIES ARE SWITCHED AS DEPICTED IN (a)-(f) (red x denotes a node point)

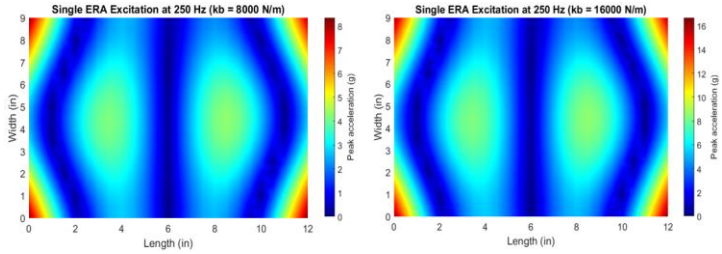

FIGURE 13: INCREASE IN INTENSITY OF VIBROTATCILE FEEDBACK WITH INCREASE IN ACTUATOR STIFFNESS (TWO DIAGONALLY OPPOSITE ERAS AT 250 HZ)

We observed an increase in vibrotactile feedback intensity with the increase in actuator stiffness, keeping the feedback pattern similar. This behavior can be observed in figure 13. In figure 13, two ERAs are activated which are diagonally opposite of each other. Both are exciting the touch surface at frequencies 250 Hz. The vibrotactile intensity increase proportionately as we increase the actuator stiffness from 8000 N/m to 16000 N/m. The increase in actuator stiffness seem to have not impacting the pattern of feedback provided on the touch surface. We seek to do a parametric study on the change in stiffness values of the ERAs and present the findings along with graphs in the final version of the paper.

4. CONCLUSION

In conclusion, the study has highlighted the potential for achieving localized haptic rendering on large TSDs through strategic switching between different excitation frequencies of the electrostatic vibration actuators considered. It is also demonstrated that the activation patterns of the multiple actuators also introduce variety in the vibrotactile haptic rendering. Combining frequency switching and the pattern of actuator activation can provide a basis for controlling the localized haptic rendering for a large TSD with a limited number of actuators. This study has also demonstrated the importance of the placement and number of actuators, and their mechanical properties like stiffness in achieving higher vibrotactile intensity on large TSDs. The results presented in the study are based on the numerical simulation of the finite-element model of a large TSD with electrostatic vibration actuators implemented in MATLAB. The modeling approach is discussed in detail. This model-based study can help in finding ways to provide rich vibrotactile feedback in large TSDs. Future extension of this study can be experimental validation of the modeling approach and the localized haptic rendering method. Further, developing controlled localized haptic rendering methods can be an interesting future research direction.

REFERENCES

[1] E. Hoggan, S. A. Brewster, and J. Johnston, "Investigating the Effectiveness of Tactile Feedback for Mobile Touchscreens," in *Proceedings of the SIGCHI conference on Human factors in computing systems*, 2008, pp. 1573–1582.

[2] T. H. Yang, J. R. Kim, H. Jin, H. Gil, J. H. Koo, and H. J. Kim, "Recent Advances and Opportunities of Active Materials for Haptic Technologies in Virtual and Augmented Reality," *Advanced Functional Materials*, vol. 31, no. 39. John Wiley and Sons Inc, Sep. 01, 2021. doi: 10.1002/adfm.202008831.

[3] K. Klein, "Rethinking Touch HMI Controls for Automotive Displays and Smart Surfaces," *Information Display*, vol. 38, no. 1, pp. 24–29, 2022.

[4] D. WANG, Y. GUO, S. LIU, Y. ZHANG, W. XU, and J. XIAO, "Haptic display for virtual reality: progress and challenges," *Virtual Reality and Intelligent Hardware*, vol. 1, no. 2, pp. 136–162, Apr. 2019, doi: 10.3724/SP.J.2096-5796.2019.0008.

[5] D. Cingel and A. M. Piper, "How parents engage children in tablet-based reading experiences: An exploration of haptic feedback," in *Proceedings of the ACM Conference on Computer Supported Cooperative Work, CSCW*, Feb. 2017, pp. 505–510. doi: 10.1145/2998181.2998240.

[6] U. von Zadow, S. Buron, T. Harms, F. Behringer, K. Sostmann, and R. Dachselt, "SimMed: Combining Simulation and Interactive Tabletopsfor Medical Ed," in *Proceedings of the SIGCHI Conference on Human Factors in Computing Systems*, 2013, pp. 1469–1478.

[7] C. H. Mejia, P. Germano, S. C. Echeverri, and Y. Perriard, "Artificial Neural Networks for Impact Position Detection in Haptic Surfaces," in *2019 IEEE International Ultrasonics Symposium (IUS)*, 2019, pp. 1874–1877.

[8] F. Sorgini, R. Caliò, M. C. Carrozza, and C. M. Oddo, "Haptic-assistive technologies for audition and vision sensory disabilities," *Disability and Rehabilitation: Assistive Technology*, vol. 13, no. 4. Taylor and Francis Ltd, pp. 394–421, May 19, 2018. doi: 10.1080/17483107.2017.1385100.

[9] S. Park, D. Kim, W. Kim, and N.-C. Park, "Rendering high-fidelity vibrotactile feedback on a plate via optimization of actuator driving signals," in *INTER-NOISE and NOISE-CON Congress and Conference Proceedings (Vol. 261, No. 6)*, 2020, pp. 548–555. [Online]. Available: https://www.ingentaconnect.com/content/ince/incecp/2020/00000261/00000006/art00066

[10] T. W. Mason, "Design and Testing of an Electrostatic Actuator with Dual-Electrodes for Large Touch Display Applications," Master's thesis, Miami University, 2021.

[11] C. Hernandez-Mejia, M. Favier, X. Ren, P. Germano, and Y. Perriard, "Reinforcement Learning and Hardware in the Loop for Localized Vibrotactile Feedback in Haptic Surfaces," in *IEEE International Ultrasonics Symposium, IUS*, 2021. doi: 10.1109/IUS52206.2021.9593749.

[12] T. Mason, J. H. Koo, Y. M. Kim, and T. H. Yang, "Experimental evaluation on the effect of electrode configuration in electrostatic actuators for increasing vibrotactile feedback intensity," *Applied Sciences (Switzerland)*, vol. 10, no. 15, Aug. 2020, doi: 10.3390/APP10155375.

[13] S. M. Rajkumar, K. V. Singh, T.-H. Yang, and J.-H. Koo, "Modeling and Experimental Evaluation of Haptic Localization Using Electrostatic Vibration Actuators," *IEEE Access*, vol. 11, pp. 18582–18589, 2023, doi: 10.1109/ACCESS.2023.3247606.

[14] S. M. Rajkumar, K. V. Singh, and J.-H. Koo, "Modeling and Analysis of Multiple Electrostatic Actuators on the Response of Vibrotactile Haptic Device," in *ASME International Mechanical Engineering Congress & Exposition IMECE October 30–November 3, 2022, Columbus, Ohio*, 2022, p.

[15] T. Mason, J. H. Koo, J. I. Kim, Y. M. Kim, and T. H. Yang, "A feasibility study of a vibrotactile system based on electrostatic actuators for touch bar interfaces: Experimental evaluations," *Applied Sciences (Switzerland)*, vol. 11, no. 15, Aug. 2021, doi: 10.3390/app11157084.

[16] J. H. Woo and J. G. Ih, "Vibration rendering on a thin plate with actuator array at the periphery," *J Sound Vib*,

vol. 349, pp. 150–162, Aug. 2015, doi: 10.1016/j.jsv.2015.03.031.

[17] C. Hudin, J. Lozada, and V. Hayward, “Localized tactile feedback on a transparent surface through time-reversal wave focusing,” *IEEE Trans Haptics*, vol. 8, no. 2, pp. 188–198, Apr. 2015, doi: 10.1109/TOH.2015.2411267.

[18] S. Wockel, U. Steinmann, and H. Arndt, “Haptics by time reversal of elastic waves,” in *IEEE International Ultrasonics Symposium (IUS)*, Mar. 2016, vol. 129, no. 3, pp. 1–3. doi: 10.1121/1.3533725.

[19] A. Ben Dhiab and C. Hudin, “Confinement of Vibrotactile Stimuli in Narrow Plates: Principle and Effect of Finger Loading,” *IEEE Trans Haptics*, vol. 13, no. 3, pp. 471–482, Jul. 2020, doi: 10.1109/TOH.2020.2986727.

[20] L. Pantera and C. Hudin, “Multitouch Vibrotactile Feedback on a Tactile Screen by the Inverse Filter Technique: Vibration Amplitude and Spatial Resolution,” *IEEE Trans Haptics*, vol. 13, no. 3, pp. 493–503, Jul. 2020, doi: 10.1109/TOH.2020.2981307.

[21] K. Katumu and J. L. Gorlewicz, “Using modal superposition for generating localized tactile effects on variable friction touchscreens,” in *IEEE Haptics Symposium, HAPTICS*, Apr. 2016, vol. 2016-April, pp. 211–216. doi: 10.1109/HAPTICS.2016.7463179.

[22] E. Enferad, C. Giraud-Audine, F. Giraud, M. Amberg, and B. L. Semail, “Generating controlled localized stimulations on haptic displays by modal superimposition,” *J Sound Vib*, vol. 449, pp. 196–213, Jun. 2019, doi: 10.1016/j.jsv.2019.02.039.

[23] B. Baylan, U. Aridogan, and C. Basdogan, “Finite element modeling of a vibrating touch screen actuated by piezo patches for haptic feedback,” in *Lecture Notes in Computer Science (including subseries Lecture Notes in Artificial Intelligence and Lecture Notes in Bioinformatics)*, 2012, vol. 7282 LNCS, no. PART 1, pp. 47–57. doi: 10.1007/978-3-642-31401-8_5.

[24] N. L. ALPDOĞAN and M. AYYİLDİZ, “Towards Localized Tactile Feedback on Touch Surfaces: Finite Element Analysis of a Vibrating Touch Screen Actuated by Piezo Patches,” *European Journal of Science and Technology*, Dec. 2021, doi: 10.31590/ejosat.1014803.

[25] A. F. Ak, G. Sari, B. M. Akgul, and B. Kirisken, “Numerical Analysis of Vibrating Touch Screen Actuated by Piezo Elements,” in *8th International Conference on Mechanical and Aerospace Engineering (ICMAE)*, 2017, pp. 775-779. IEEE.

[26] R. Le Magueresse *et al.*, “Piezoelectric flexible haptic interface development,” in *23rd International Conference on Thermal, Mechanical and Multi-Physics Simulation and Experiments in Microelectronics and Microsystems (EuroSimE)*, 2022, pp. 1-5. IEEE. doi: 10.1109/EuroSimE54907.2022.9758912.

[27] S. S. Rao, *Vibration of continuous systems*. John Wiley & Sons, 2019.

[28] R. Baušys, “Free vibration analysis of reissner-mindlin plates by a modified linked interpolation element,” *Statyba*, vol. 5, no. 2, pp. 83–90, Jan. 1999, doi: 10.1080/13921525.1999.10531441.